Journal of Modern Optics
Vol. 57, No. 18, 20 October 2010, 1731–1737

Taylor & Francis
Taylor & Francis Group

Near-infrared image formation and processing for the extraction of hand veins

Nabila Bouzida*, Abdel Hakim Bendada and Xavier P. Maldague

Computer Vision and Systems Laboratory, Laval University, Quebec City G1V 0A6, Canada

(*Received 28 December 2009; final version received 16 February 2010*)

The main objective of this work is to extract the hand vein network using a non-invasive technique in the near-infrared region (NIR). The visualization of the veins is based on a relevant feature of the blood in relation with certain wavelengths of the electromagnetic spectrum. In the present paper, we first introduce the image formation in the NIR spectral band. Then, the acquisition system will be presented as well as the method used for the image processing in order to extract the vein signature. Extractions of this pattern on the finger, on the wrist and on the dorsal hand are achieved after exposing the hand to an optical stimulation by reflection or transmission of light. We present meaningful results of the extracted vein pattern demonstrating the utility of the method for a clinical application like the diagnosis of vein disease, of primitive varicose vein and also for applications in vein biometrics.

Keywords: near-infrared imaging; biometrics; mathematical morphology; image processing; feature extraction; anisotropic diffusion

1. Introduction

The near-infrared region (NIR) is situated in the electromagnetic spectrum between the visible region and the mid-wave infrared region (MWIR). The American Society for Testing and Materials (ASTM) has defined it as the spectral area extending between 780 and 2500 nm [1]. However, many applications using these waves for biometrics or medical applications are carried out between 780 and 950 nm. The use of NIR light for clinical applications was initiated in 1988 by the work of Cope and Delpy [2]. Their research had a great impact and was focused on the measurement of blood oxygenation in the brain of premature babies.

Blood consists of lipids, nutritive components, proteins and 95% water. Thus, water is the dominant element of the human tissue and it is known for its high absorption of photons in the wavelengths between 300 and 1000 nm [3]. Moreover, the most absorbing protein of NIR light is haemoglobin. Hence, while using a NIR illuminator in this spectral band, the highest absorption of this illumination is principally inherent to the veins. Because of the low absorption of skin and subcutaneous tissue in the NIR-wavelength range, the NIR light penetrates these tissues effectively. NIR light is absorbed or scattered in the forward direction by blood, whereas it is scattered in skin and subcutaneous fat [4]. Therefore, blood appears as a dark region, whereas skin and fat appear lighter. This specificity brings us to use NIR light and some image processing tools in order to extract the venous structure of the hand.

1.1. The acquisition system

For the purpose of this study, a Phoenix Monochrome Camera, Model PC-1280 (MuTech Corporation, North Billerica, MA, USA) was employed. This camera has been chosen first of all for its high sensitivity to NIR light. In addition, it is a relatively small portable camera with a spatial resolution attaining 1280×1024 pixels. Figure 1 shows its spectral sensitivity. Moreover, in order to be able to measure the NIR light, an infrared cut-off filter was removed from the camera.

The experimental setup used to obtain the vein network is illustrated in Figure 2. It shows an example of visualization of the finger vein network using a light projected by an infrared illuminator and transmitted through the tissue. There are two different infrared projectors available in our laboratory, emitting in 850 and 940 nm. Images obtained with the 850 nm show a better contrast, despite the higher power of the 940 nm illuminator. This is mainly due to the spectral sensitivity of the camera, which is greater around 850 nm, as shown in Figure 1.

*Corresponding author. Email: nbouzida@gel.ulaval.ca

ISSN 0950–0340 print/ISSN 1362–3044 online

DOI: 10.1080/09500341003725763
http://www.informaworld.com

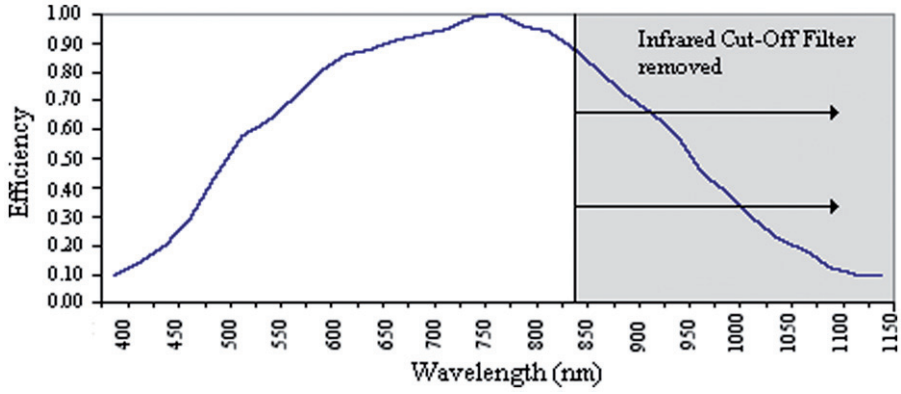

Figure 1. Spectral sensitivity of the Mutech camera. (The color version of this figure is included in the online version of the journal.)

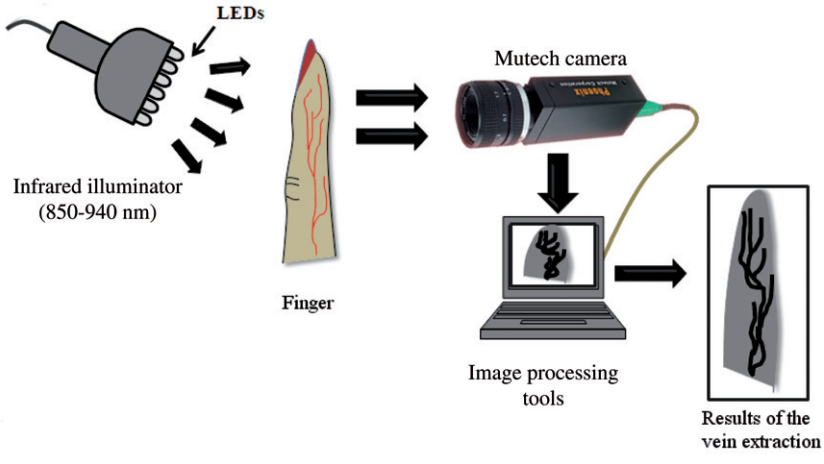

Figure 2. The experimental setup. Illustration of the light transmission through the finger. (The color version of this figure is included in the online version of the journal.)

The NIR light emitted by the optical stimulation is partially absorbed, diffused or reflected, according to the analyzed tissue layer. In order to capture only the NIR light, we inserted a visible cut-off filter in the optical path of the camera. Three (3) stimulation techniques can be carried out in order to inspect a specimen in the NIR spectral region: by *transmission*, *reflection* or *transflection*.

After carrying out a few experiments for the purpose of this study, it was concluded that a better visualization of the veins on the dorsal hand is made possible by light reflection. This is due to the large surface and thickness of the hand. As for the visualization of the finger venous network, it is more relevant to use the transmission of light through the fingers.

The infrared light is partially absorbed by the hemoglobin, with a difference depending on whether it is saturated with oxygen (HbO_2) or not (Hb). Thus, the areas just above the blood vessels appear darker than the surrounding areas. In the following subsections, the chosen modes for the visualization of the vein pattern are described.

1.2. The reflection mode

In the reflection mode, the infrared illuminator of 850 nm and the camera are placed side by side in front of the hand. The camera, which is sensitive to this wavelength, captures the reflected light from the hand. Figure 3 shows an example of a vein tree of the wrist visualized in the NIR region after light reflection.

1.3. The transmission mode

In this mode, the fingers are placed between the camera and the infrared illuminator of 850 nm. Light passes through the fingers after successive diffusions.

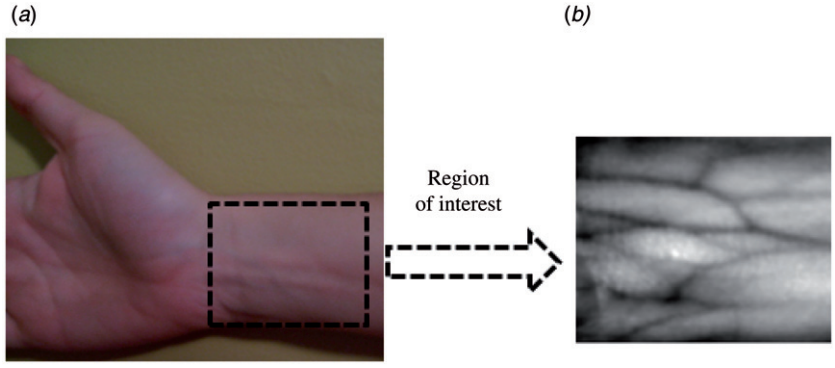

Figure 3. (*a*) Visible image, and (*b*) vein pattern obtained by light reflection on the wrist area. (The color version of this figure is included in the online version of the journal.)

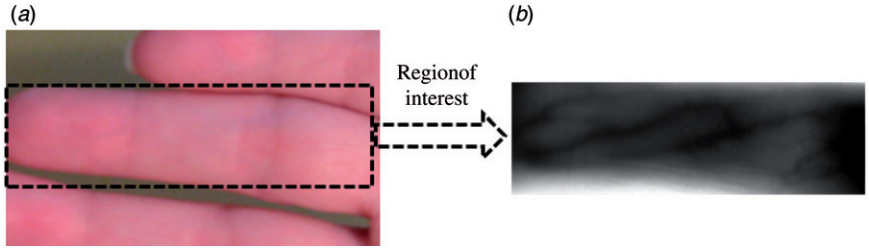

Figure 4. (*a*) Visible image, and (*b*) vein pattern on the image obtained by light transmission through the fingers. (The color version of this figure is included in the online version of the journal.)

The NIR illuminator is placed at a 45° angle to the surface normal (Figure 2) in order to prevent the light from passing in between the fingers directly towards the camera. Consequently, local saturations in the images are avoided. Figure 4 shows a typical example of visualization after light transmission through the fingers.

2. Image processing

The images recorded in the NIR contain not only the venous structure that we want to extract, but also some fuzzy areas representing the osseous forms, shades and some wrinkles.

2.1. *Normalization of the illumination in the NIR image*

When using an optical stimulation in order to obtain a contrast between the vein and the surrounding area, a non-uniformity of illumination is observed in the images.

To reduce this light effect, an algorithm based on the normalization of the local mean and the standard deviation in the image is applied taking into account the statistical properties of neighbor pixels. At the same time, this normalization is also useful to eliminate the effect of shades.

The mean μ and the standard deviation σ are first estimated with a Gaussian kernel by choosing a pixel neighbourhood region of 5×5 (Equations (1) and (2)):

$$\mu = \frac{1}{N \times M} \sum_{x=0}^{N-1} \sum_{y=0}^{M-1} I(x, y), \tag{1}$$

$$\sigma^2 = \frac{1}{N \times M} \sum_{x=0}^{N-1} \sum_{y=0}^{M-1} (I(x, y) - \mu)^2, \tag{2}$$

where $I(x, y)$ is the intensity of the pixel (x, y) and $N \times M$ is the size of the original image. The σ value indicates the distribution of light intensity throughout the image. In this case, the resulting image $J(x, y)$ is given by the operations in Equation (3), processing in detail the neighborhood of each pixel. In this case, the resulting image $J(x, y)$ is given by the following operations (Equation (3)), processing in detail the neighbourhood of each pixel.

$$J(x, y) = \begin{cases} \mu_d + \left(\dfrac{\sigma_d^2 (I(x, y) - \mu)^2}{\sigma^2} \right)^{1/2}, & \text{if } I(x, y) > \mu, \\ \mu_d - \left(\dfrac{\sigma_d^2 (I(x, y) - \mu)^2}{\sigma^2} \right)^{1/2}, & \text{if } I(x, y) \leq \mu, \end{cases} \tag{3}$$

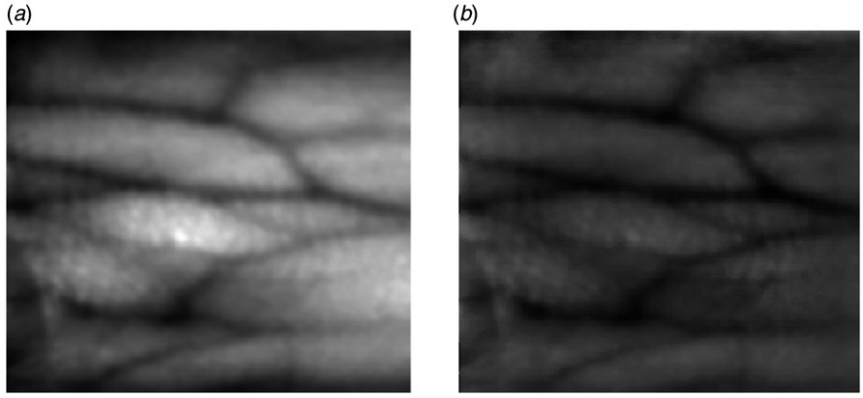

Figure 5. (*a*) NIR image of the wrist, and (*b*) image after processing of the non-uniformity of light.

where μ_d and σ_d are, respectively, the desired mean and standard deviation after normalization for the whole image. Hong et al. [5] were the first to use this technique for the normalization of the digital fingerprints. Figure 5 shows an example of processing based on the normalization of the non-uniformity in the image.

2.2. *Anisotropic diffusion for the image smoothing and contrast enhancement*

The objective of this filtering is to carry out a preliminary smoothing of the images without destroying the edges but on the contrary, to preserve them. In fact, these edges represent principally the vein curves that we want to extract. Therefore, it is very important to smooth the regions that surround the veins and enhance those representing the vein structure.

The anisotropic diffusion (AD) is a processing tool that uses a nonlinear filter for the smoothing of the images [6]. In this technique, the smoothing is formulated as a diffusive process and it is stopped on boundaries by choosing locally adaptive diffusion power. This means that the AD filtering uses a variable diffusion coefficient C in the heat equation that depends upon the magnitude of the gradient (Equation (4)).

$$\partial I_t = \frac{\partial}{\partial t} I(\bar{x}, t) = \mathrm{div}(C(\bar{x}, t)\, \nabla I(\bar{x}, t)), \tag{4}$$

where ∇ is the gradient operator, I is the intensity at the spatial coordinates $\bar{x} = (x, y)$, whereas t represents the time-step. In this case, ∂I_t determines the modification of the image dependent on the time t. To achieve this diffusion, a decreasing non-linear and non-negative function is used according to the Perona and Malik model [7]. In this study, we have chosen the coefficient given in Equation (5), which verifies all the properties of this function.

$$C(\bar{x}, t) = \frac{1}{1 + \left(\left\|\nabla I(\bar{x}, t)\right\|/K\right)^2}. \tag{5}$$

The value ∇I is calculated by building the difference of two intensity values from each side of the edge [6]. The flow constant K is used to control the desired diffusion speed and it obviously has a great influence on the filter. In order to understand this process, a flow function is introduced as follows:

$$\Phi(\bar{x}, t) = C(\bar{x}, t)\nabla I(\bar{x}, t). \tag{6}$$

The flow increases when $\|\nabla I\|$ approaches K and then decreases to zero. Moreover, where $\|\nabla I\| \ll K$, homogeneous intensity areas in the image are kept since little flow is produced. In a similar way, where $\|\nabla I\| \gg K$, the edges are preserved because the flow is small. Conversely, the greatest flow is produced where $\|\nabla I\| \approx K$. Therefore, edges can be enhanced when K is selected slightly less than the gradient magnitude of the edges.

In summary, when we are in the presence of low values of the gradient, the diffusion is made with a high diffusion coefficient. On an area characterized by a strong gradient, the diffusion is lessened by a low diffusion coefficient. Furthermore, the flow of the Perona–Malik diffusivity model reaches its maximum at $\|\nabla I\| = K/2^{1/2}$ [6]. Figure 6 is an illustration of the results obtained after the smoothing with this method.

2.3. *Morphological operations*

The morphological operations that we applied for the extraction of the vein pattern use the principles of image opening and closing [8]. These two standard techniques are used to obtain the Top-Hat and the

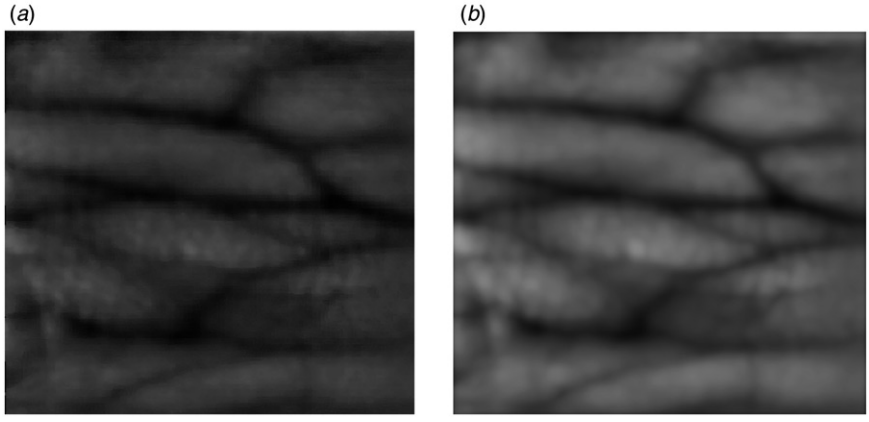

Figure 6. (*a*) Image of the AD filtering, and (*b*) processed image using the AD with a diffusion constant $K = 0.4$ and 18 iterations.

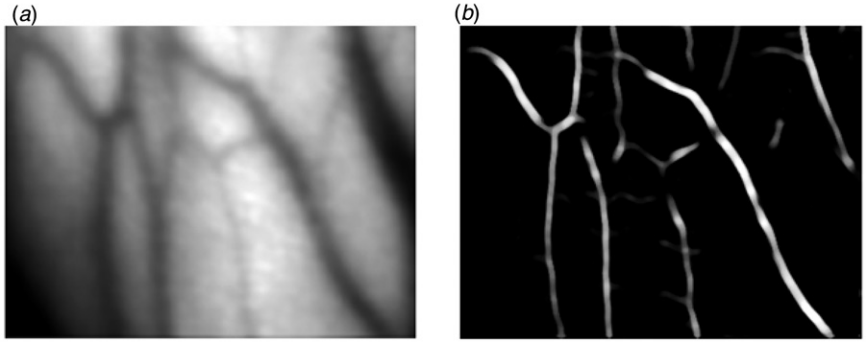

Figure 7. (*a*) NIR image of the dorsal hand, and (*b*) vein pattern extraction.

Bottom-Hat images, which are defined in the following [8]:

- To detect light objects: $\text{TopHat}(A, B) = A - (A \circ B)$;
- To detect dark objects: $\text{BottomHat}(A, B) = (A \bullet B) - A$.

The aim of these operations is to detect contrasted objects in an image with a non-uniform background. Sometimes, these two transformations also compensate for the difficulties of image thresholding in the presence of non-uniform illumination. These mathematical operations on the image use a structural element B for the image A, where $(A \circ B)$ is the image opening and $(A \bullet B)$ the image closing. Structuring elements B can be selected according to the shapes that we want to extract. In our case, we have chosen a disk element with a diameter close to the diameter of the curve (vein). The algorithm is summarized as follows:

Step 1: Original image I_0 – its Opening = Top-Hat (I_{TH})
Step 2: $I_{\text{TH}} + I_0 = I_{\text{EC}}$ (Enhanced Contrast)
Step 3: Closing of image $I_0 - I_0 =$ Bottom-Hat (I_{BH})
Step 4: Top-Hat of $(I_{\text{EC}} - I_{\text{BH}}) = I_{\text{result}}$
Step 5: Thresholding of I_{result}.

2.4. *Results of the vein extraction obtained in the reflection mode*

We notice from Figures 7 and 8 that the extraction obtained perfectly respects the lines of the veins in the infrared image. However, in the case of the dorsal hand vein pattern, some small and thin curves representing wrinkles on the hand still remain even after the processing.

2.5. *Results of the vein extraction obtained in the transmission mode*

One more result that we want to present is the extraction of the venous network on the finger. Figure 9 illustrates a venous pattern which is well

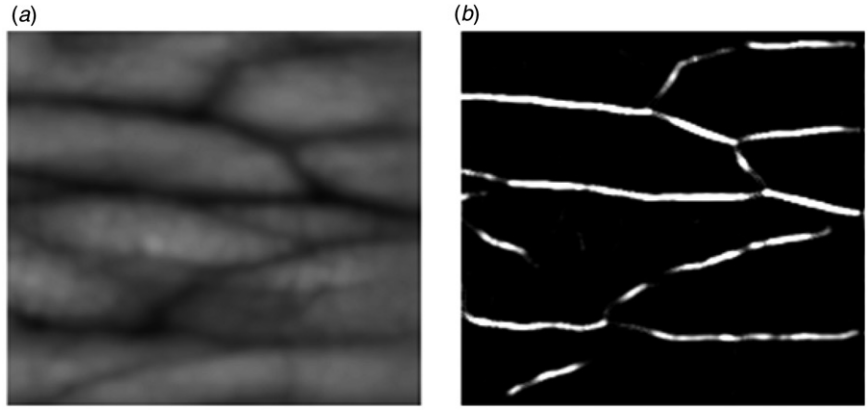

Figure 8. (*a*) NIR image of the wrist, and (*b*) vein pattern extraction.

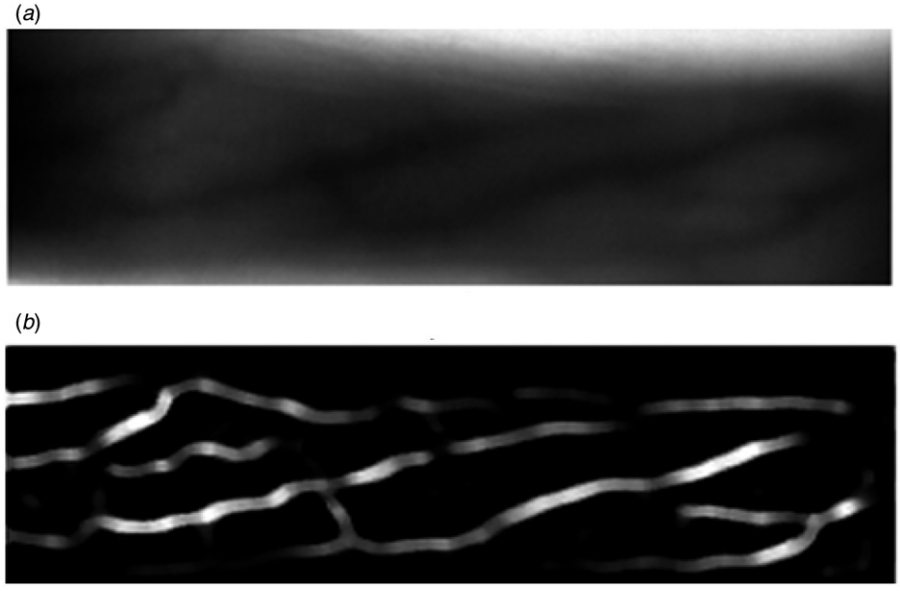

Figure 9. (*a*) NIR image of the finger, and (*b*) vein pattern extraction.

characterized by the use of the appropriate processing tools.

3. Conclusion

We have shown in this paper the utility of NIR light for the visualization of the vein structure in the subcutaneous layer of the skin. Two different modes are examined. After several experiments, it was concluded that for a better visualization of the finger vein structure, a transmission of light through the fingers gives more compelling results, whereas the light reflection mode is chosen to visualize areas on the dorsal hand and on the wrist.

The NIR images have shown dark curves representing the vascular tree. They also show a constant noise related to the optical stimulation and to other structures of the skin (wrinkles, shades of the osseous region, etc.). Therefore, we normalized the illumination in the image by estimating the mean and the standard deviation. Then we applied an AD filter in order to smooth the areas of the image depending on the intensity gradient, encouraging intra-region smoothing while inhibiting inter-region smoothing. The destruction of the edges representing the vein curves is avoided by setting a variable diffusion coefficient. The Top-Hat and Bottom-Hat techniques were used finally in order to extract the venous network from the background.

The results are very encouraging since the venous pattern represents the structure of the vein in the NIR image well. It is also important to emphasize that a great advantage of this method is the fact that it is

non-invasive and that it could help clinicians to efficiently locate the veins during intravenous injections. Future works will be focused on the improvement of the acquisition system in order to diminish the artifacts caused principally by the light illumination.

Acknowledgements

The authors are grateful to the Multipolar Infrared Vision Chair MiViM, funded by the Natural Sciences and Engineering Research Council of Canada (NSERC).

References

[1] The American Society for Testing and Materials, *Standard Practices for Infrared Multivariate Quantitative Analysis*. http://www.astm.org/Standards/E1655.htm (accessed Oct 20, 2009).

[2] Cope, M.; Delpy, D.T. *Med. Biol. Eng. Comp.* **1988,** *26,* 289–294.

[3] Burns, D.A.; Ciurczak, E.W. *Handbook of Near-Infrared Analysis*, Practical Spectroscopy Series, 3rd ed.; CRC Press: Boca Raton, FL, 2008; Vol. 35.

[4] Miyake, R.K.; Zeman, H.D.; Duarte, F.H.; Kikuchi, R.; Ramacciotti, E.; Lovhoiden, G.; Vrancken, C. *Dermatol. Surg*. **2006,** *32,* 1031–1038.

[5] Hong, L.; Wan, L.Y.; Jain, A. *IEEE T. Pattern Anal.* **1998,** *20,* 777–789.

[6] Fritz, L. Diffusion-Based Applications for Interactive Medical Image Segmentation. *Proceedings of the 10th Central European Seminar on Computer Graphics (CESCG 2006)*, Slovakia, April 24–26, 2006.

[7] Perona, P.; Malik, J. *IEEE T. Pattern Anal.* **1990,** *12,* 629–639.

[8] Dougherty, E.R.; Lotufo, R.A. Hands-on Morphological Image Processing. *SPIE Tutorial Texts in Optical Engineering*; SPIE Press: Bellingham, WA, 2003; Vol. TT59.